IOP Publishing Physica Scripta
Phys. Scr. 95 (2020) 035102 (6pp) https://doi.org/10.1088/1402-4896/ab553e

# Measuring weak magnetic field via dissipatively coupled opto-mechanical system

**Asad Mehmood[1], Sajid Qamar[2] and Shahid Qamar[1,3,4]**

[1] Department of Physics and Applied Mathematics, Pakistan Institute of Engineering and Applied Sciences (PIEAS), Nilore, Islamabad 45650, Pakistan
[2] Quantum Optics Lab, Department of Physics, COMSATS University, Islamabad, Pakistan
[3] Center for Mathematical Sciences, PIEAS, Nilore, Islamabad, Pakistan

E-mail: shahid_qamar@pieas.edu.pk

Received 12 July 2019, revised 29 October 2019
Accepted for publication 7 November 2019
Published 28 January 2020

**Abstract**

In this paper, we propose a scheme for the detection of weak magnetic field based on dissipatively coupled optomechanical system. The system considered here is composed of a perfect mirror and a compound mirror formed by a Michelson–Sagnac interferometer (MSI) with a movable membrane. When the transmissivity of MSI is close to zero, it sensitively depends upon the position of membrane. Under this condition, the two mirrors results in an effective Fabry–Perot interferometer (FPI) whose linewidth depends upon the position of the membrane. We show that by applying current to the membrane in the presence of magnetic field, the position of the membrane changes which in turn changes the linewidth of the effective FPI. This change can be observed in the spectrum of the output field and consequently enables us to measure weak magnetic field. Thus an optical detection technique is proposed for the detection of weak magnetic field.

Keywords: dissipatively coupled optomechanical system, Michelson–Sagnac interferometer, measure weak magnetic

(Some figures may appear in colour only in the online journal)

## 1. Introduction

Optomechanical systems are providing potential applications in precision measurements. They can be used to achieve sensitivity beyond the standard quantum limit in gravitational wave detectors [1–5], as a quantum speed meter [6–8], torque sensor [9], magnetometer [10, 11] and in precision measurement of electric charge [12]. In optomechanical cavities, light inside the cavity couples with the mechanical modes of the oscillator in two different ways. When the displacement of the mechanical oscillator changes the resonance frequency of the cavity, it leads to the so called dispersive coupling. And when the displacement of the mechanical oscillator modulates the linewidth of the cavity, it leads to dissipative coupling. A lot of work has been done in dispersively coupled optomechanical system, however, it has its own constraints e.g. requirement of side-band resolved regime for ground state cooling [13, 14] which is not always feasible particularly in the case of low mechanical frequencies. However, such requirements are not necessary for dissipatively coupled optomechanical cavities [15–19]. Dissipatively coupled optomechanical systems are also studied for normal mode splitting [20], electromagnetically induced transparency [20, 21], squeezing of output light [22, 23], quantum speed meter [8] and force sensing [24].

The precision measurement of weak magnetic field has gained a lot of interest due to its practical application in various fields like geology, material characterization and medicine [25]. Magnetometers based on superconducting quantum interference devices operating at cryogenic

[4] Author to whom any correspondence should be addressed.

 

temperatures, magnetostrictive magnetometers and atomic magnetometers provides remarkable sensitivity [26–30]. In recent studies, the magnetic field sensors based on optomechanical cavity were also proposed, they have small size, high sensitivity and operational capability at room temperature [10, 31]. In another study, a technique based on optomechanical induced transparency was proposed for the detection of weak magnetic fields [11].

In this paper, we present an optical detection technique for measuring weak magnetic field which can work at room temperature. We use a dissipatively coupled optomechanical system that can be realized in a Michelson–Sagnac interferometer (MSI) with a movable membrane [15–17]. MSI can be considered as a compound mirror as the position of the movable membrane sensitively affects the transmissivity of MSI when it operates close to the dark port condition. Under this condition, the compound MSI mirror along with a perfect mirror forms an effective Fabry–Perot interferometer (FPI) whose linewidth depends upon the position of the membrane. In addition, when current is applied to the membrane in the presence of a magnetic field, it leads to the magnetic coupling of the membrane which directly affects the linewidth of the effective FPI. As a result, the output spectrum of the field is affected and therefore, enables measurement of weak magnetic field. Interestingly, magnetic field as low as 0.1 nT can be measured by this scheme. The paper is organized as follows. In section 2, we present our model and solve the equations of motion. We find an expression for the output quadrature of the field and calculate the spectral density. In section 3, we present results of our numerical calculations. Finally, in section 4, we conclude our results.

## 2. Theory and model

We consider an optomechanical system where a mechanical resonator of effective mass $m$ and resonance frequency $\omega_m$ is dissipatively coupled to a cavity field with eigenfrequency $\omega_o$. The cavity is driven with a strong coherent light of frequency $\omega_l = \omega_o$ and amplitude $\varepsilon_l$. In a frame rotating at input laser frequency $\omega_l$, the Hamiltonian of the system is given by

$$\hat{H} = \left(\frac{p^2}{2m} + \frac{1}{2}m\omega_m^2 x^2\right) + \hbar(\omega_o - \omega_l)c^\dagger c + \mathrm{i}\hbar\sqrt{2\kappa}\,[\varepsilon_l(c^\dagger - c) + c^\dagger c_{\mathrm{in}} - c_{\mathrm{in}}^\dagger c] + \zeta B x, \qquad (1)$$

where the first term describes the energy of the mechanical oscillator (MO) with $x$ and $p$ being the position and momentum operators satisfying the commutation relation $[x, p] = \mathrm{i}\hbar$. The second term is the free energy of the cavity field. The third term represents the coupling of cavity field with the input laser and input vacuum noise represented by $c_{\mathrm{in}}$. The last term represents the magnetic coupling of the MO where $\zeta$ is the current coefficient or magnetic coupling coefficient. It may also be noted that $\kappa = \kappa_o(1 + \eta x)$ represents the position dependent photon decay rate or linewidth of the cavity and $\kappa_o$ is the photon decay rate when $x = 0$. It is related to the dissipative coupling strength $g_\kappa$ such that $g_\kappa = x_{zpf}\mathrm{d}\kappa/\mathrm{d}x$

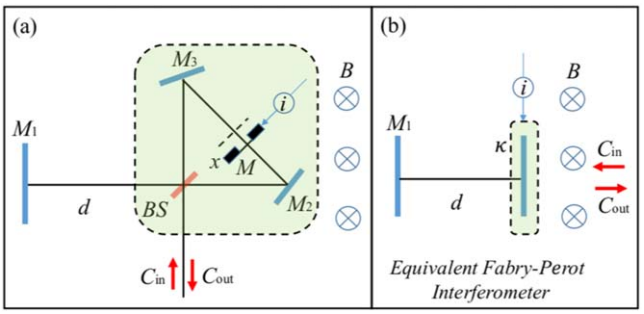


**Figure 1.** The schematics of the system. (a) A Michelson–Sagnac interferometer, containing the membrane $M$ through which current $i$ is flowing. The membrane is displaced from its mean position due to radiation pressure and external magnetic field $B$. (b) Equivalent Fabry–Perot interferometer whose right mirror transmission depends upon the decay rate $\kappa$.

where $x_{zpf} = \sqrt{\hbar/2m\omega_m}$ is the zero point fluctuation of the membrane. Therefore, $g_\kappa = \eta\ \kappa_o x_{zpf}$, represents the dissipative coupling constant between the cavity field and MO which depends upon $\eta$. The parameter $\eta$ is related to the power reflectivity of the membrane and beam-splitter asymmetry [17]. The amplitude of the field is related to the input power $P$ as $\varepsilon_l = \sqrt{P/\hbar\omega_l}$.

The schematics of the system is shown in figure 1. It is assumed that the current is passing through the movable membrane $M$ of MSI and the whole system is placed in a static magnetic field. The mean position of the membrane changes due to magnetic coupling of the membrane. The entire setup is equivalent to a FPI with the variable optical decay rate i.e. $\kappa = \kappa_o(1 + \eta x)$, where $x$ is the displacement of the membrane. The displacement of the membrane can be controlled by the application of current in the presence of a magnetic field. Thus the right mirror of the effective FPI has optical transmissivity that depends upon the current in the presence of magnetic field.

The Heisenberg equations of motion for the system when the cavity mode is resonantly pumped by the input laser (i.e. $\omega_o = \omega_l$) are given by the following:

$$\begin{aligned}
\dot{x} &= \frac{p}{m},\\
\dot{p} &= -\frac{\mathrm{i}\hbar\eta\sqrt{2\kappa_o}}{2}[\varepsilon_l(c^\dagger - c) + c^\dagger c_{\mathrm{in}} - c_{\mathrm{in}}^\dagger c]\\
&\quad - m\omega_m^2 x - \zeta B - \gamma_m p + \xi,\\
\dot{c} &= \sqrt{2\kappa_o}\left(1 + \frac{\eta}{2}x\right)(\varepsilon_l + c_{\mathrm{in}}) - \kappa_o(1 + \eta x)c, \qquad (2)
\end{aligned}$$

where $\gamma_m$ is the mechanical damping rate and $\xi$ is the zero mean value thermal noise which describes the coupling of MO to the thermal environment. It follows immediately from equation (2) that in steady-state, the position, momentum and cavity field must fulfill the following self consistent equations:

$$p_s = 0,\ x_s = -\frac{\zeta B}{m\omega_m^2},\ c_s = \frac{\sqrt{2\kappa_o}(1 + \eta x_s/2)\varepsilon_l}{\kappa_o(1 + \eta x_s)}. \qquad (3)$$

The operators given by equation (2) can be represented as a sum of large mean value and small fluctuating terms such that $x = x_s + \delta x$, $p = p_s + \delta p$ and $c = c_s + \delta c$. In the first order approximation, the linearized equations of motion are given by

$$\begin{aligned}
\delta\dot{x} &= \frac{\delta p}{m},\\
\delta\dot{p} &= -\frac{\mathrm{i}\hbar\eta\sqrt{2\kappa_o}}{2}[\varepsilon_l(\delta c^{\dagger} - \delta c) + c_s(c_{\mathrm{in}} - c_{\mathrm{in}}^{\dagger})]\\
&\quad - m\omega_m^2\delta x - \gamma_m\delta p + \xi,\\
\delta\dot{c} &= -\kappa_o(1 + \eta x_s)\delta c - \frac{\kappa_o\eta c_s}{2(1 + \eta x_s/2)}\delta x\\
&\quad + \sqrt{2\kappa_o}(1 + \eta x_s/2)c_{\mathrm{in}}.
\end{aligned} \tag{4}$$

By taking Fourier transform of equation (4), the cavity field and position fluctuation in frequency domain can be written as:

$$\begin{aligned}
\delta c(\omega) &= \frac{1}{\kappa_o(1 + \eta x_s/2) - \mathrm{i}\omega}\\
&\quad \times\left\{-\frac{\kappa_o\eta c_s}{2(1 + \eta x_s/2)}\delta x + \sqrt{2\kappa_o}(1 + \eta x_s/2)c_{\mathrm{in}}\right\},\\
\delta x(\omega) &= \frac{1}{m[\omega_m^2 - \omega^2 - \mathrm{i}\omega\gamma_m]}\\
&\quad \times\left\{\xi - \frac{\hbar\eta\sqrt{2\kappa_o}\,\omega c_s}{2[\kappa_o(1 + \eta x_s) - \mathrm{i}\omega]}(c_{\mathrm{in}} - c_{\mathrm{in}}^{\dagger})\right\}.
\end{aligned} \tag{5}$$

The output field of the system and its fluctuation can be found by the input output formalism [32]:

$$\begin{aligned}
c_{\mathrm{out}} &= -c_{\mathrm{in}} + \sqrt{2\kappa}\,c,\\
\delta c_{\mathrm{out}}(\omega) &= -c_{\mathrm{in}}(\omega) + \sqrt{2\kappa_o}\,\delta c(\omega) + \sqrt{2\kappa_o}\,\frac{\eta c_s}{2}\delta x(\omega).
\end{aligned} \tag{6}$$

The output field of the system can be found by substituting equations (5) in (6), i.e.

$$\begin{aligned}
\delta c_{\mathrm{out}}(\omega) &= \left[\frac{2\kappa_o(1 + \eta x_s/2)}{\kappa_o(1 + \eta x_s) - \mathrm{i}\omega} - 1\right]c_{\mathrm{in}}\\
&+ \left[1 - \frac{\kappa_o}{[\kappa_o(1 + \eta x_s) - \mathrm{i}\omega](1 + \eta x_s/2)}\right]\frac{\sqrt{2\kappa_o}\,\eta c_s\delta x}{2}.
\end{aligned} \tag{7}$$

Next we define the input amplitude and phase quadratures as $X_{\mathrm{in}}(\omega) = \frac{1}{\sqrt{2}}[c_{\mathrm{in}}(\omega) + c_{\mathrm{in}}^{\dagger}(\omega)]$ and $Y_{\mathrm{in}}(\omega) = \frac{1}{i\sqrt{2}}[c_{\mathrm{in}}(\omega) - c_{\mathrm{in}}^{\dagger}(\omega)]$. Similarly, the output field's amplitude and phase quadratures are defined as $X_{\mathrm{out}}(\omega) = \frac{1}{\sqrt{2}}[\delta c_{\mathrm{out}}(\omega) + \delta c_{\mathrm{out}}^{\dagger}(\omega)]$ and $Y_{\mathrm{out}}(\omega) = \frac{1}{i\sqrt{2}}[\delta c_{\mathrm{out}}(\omega) - \delta c_{\mathrm{out}}^{\dagger}(\omega)]$. On substituting the values of $\delta c_{\mathrm{out}}(\omega)$ and $\delta c_{\mathrm{out}}^{\dagger}(\omega)$, the output quadratures of the field are found to be:

$$\begin{aligned}
X_{\mathrm{out}} &= \frac{\kappa_o + \mathrm{i}\omega}{\kappa_o(1 + \eta x_s) - \mathrm{i}\omega}[X_{\mathrm{in}} + \alpha_1 Y_{\mathrm{in}} - \alpha_2\xi],\\
Y_{\mathrm{out}} &= \frac{\kappa_o + \mathrm{i}\omega}{\kappa_o(1 + \eta x_s) - \mathrm{i}\omega}Y_{\mathrm{in}},
\end{aligned} \tag{8}$$

where $\alpha_1$ and $\alpha_2$ are defined as

$$\begin{aligned}
\alpha_1 &= \frac{\mathrm{i}J\kappa_o^2\chi\omega[\kappa_o - (1 + \eta x_s/2)\{\kappa_o(1 + \eta x_s) - \mathrm{i}\omega\}]}{\omega_m(\kappa_o + \mathrm{i}\omega)(1 + \eta x_s/2)\{\kappa_o(1 + \eta x_s) - \mathrm{i}\omega\}},\\
\alpha_2 &= \sqrt{\frac{J}{m\hbar}}\,\frac{\chi[\kappa_o - (1 + \eta x_s/2)\{\kappa_o(1 + \eta x_s) - \mathrm{i}\omega\}]}{\omega_m(\kappa_o + \mathrm{i}\omega)(1 + \eta x_s/2)},
\end{aligned} \tag{9}$$

with $J = \hbar\eta^2 c_s^2/m\kappa_o$, being the dimensionless power and $\chi = \omega_m/(\omega_m^2 - \omega^2 - \mathrm{i}\omega\gamma_m)$ is the mechanical susceptibility. The output field can also be expressed as $Z_{\mathrm{out}}(\omega) = X_{\mathrm{out}}(\omega)\cos\theta + Y_{\mathrm{out}}(\omega)\sin\theta$, where $\theta$ represents the homodyne phase angle. We obtained the following expression for the generalized quadrature:

$$\begin{aligned}
Z_{\mathrm{out}}(\omega) &= \frac{(\kappa_o + \mathrm{i}\omega)\cos\theta}{\kappa_o(1 + \eta x_s) - \mathrm{i}\omega}\\
&\quad \times[X_{\mathrm{in}} + (\alpha_1 + \tan\theta)Y_{\mathrm{in}} - \alpha_2\xi].
\end{aligned} \tag{10}$$

Using the correlation functions of the input vacuum and thermal noise

$$\begin{aligned}
\langle X_{\mathrm{in}}(\omega)X_{\mathrm{in}}(\omega')\rangle &= \langle Y_{\mathrm{in}}(\omega)Y_{\mathrm{in}}(\omega')\rangle = \frac{1}{2}2\pi\delta(\omega + \omega'),\\
\langle X_{\mathrm{in}}(\omega)Y_{\mathrm{in}}(\omega')\rangle &= -\langle Y_{\mathrm{in}}(\omega)X_{\mathrm{in}}(\omega')\rangle = \frac{\mathrm{i}}{2}2\pi\delta(\omega + \omega'),\\
\langle\xi(\omega)\xi(\omega')\rangle &= 4\pi mk_BT\gamma_m\delta(\omega + \omega'),
\end{aligned} \tag{11}$$

the spectrum of the fluctuation in the quadrature $Z_{\mathrm{out}}(\omega)$ of the output field can be written as

$$\begin{aligned}
&\frac{1}{2}[\langle Z_{\mathrm{out}}(\omega)Z_{\mathrm{out}}(\omega')\rangle + \langle Z_{\mathrm{out}}(\omega')Z_{\mathrm{out}}(\omega)\rangle]\\
&\quad = 2\pi S_{\mathrm{out}}(\omega)\delta(\omega + \omega').
\end{aligned} \tag{12}$$

The spectral density of the output field is found to be:

$$\begin{aligned}
S_{\mathrm{out}}(\omega) &= \frac{(\kappa_o^2 + \omega^2)\cos^2\theta}{2[\kappa_o^2(1 + \eta x_s)^2 + \omega^2]}\\
&\quad \times[1 + |\alpha_1 + \tan\theta|^2 + 4mk_BT\gamma_m|\alpha_2|^2].
\end{aligned} \tag{13}$$

In equation (13), the first term is the contribution from the photons shot noise, the second term is from the back-action and the last term is from the thermal noise. The homodyne phase angle $\theta$ can also be optimized to supress the back action term. This can be done by setting the homodyne angle $\theta$ such that $\tan\theta_{\mathrm{opt}} = -\alpha_1$.

## 3. Results and discussion

In this section, we present the results of our numerical simulation. Here, we consider $m = 50$ pg, $\kappa_o = 2\pi \times 59$ KHz, $\lambda = 1064$ nm, $g_k = 2\pi \times 2.6$ Hz, $Q = \omega_m/\gamma_m = 1.1 \times 10^7$, $T = 300$ K and $\omega_m \sim \kappa_o$ (i.e. non-resolved-sideband regime) as discussed in [16, 33–35]. It may also be noted that SiN membrane coated with Aluminium or Graphene [36, 37] can be used for realization of current flowing through the membrane. As we discussed earlier, in the presence of magnetic field, the transmissivity of the right mirror of the effective FPI depends upon the current flowing through it. Therefore, a shift in the output spectral density of the field

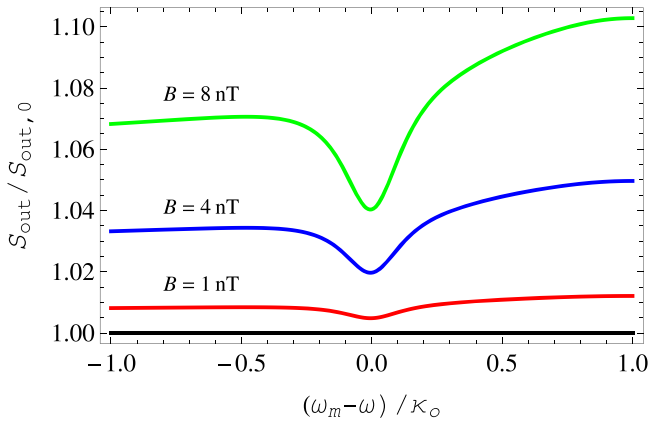


**Figure 2.** Normalized spectral density of the output field when $B = 0$ (straight line at $S_{out}/S_{out,0} = 1$), which becomes greater than 1 for $B \neq 0$. Here the parameters $m = 50$ pg, $\kappa_o = 2\pi \times 59$ KHz, $\lambda = 1064$ nm, $g_k = 2\pi \times 2.6$ Hz, $Q = \omega_m/\gamma_m = 1.1 \times 10^7$, $\omega_m \sim \kappa_o$, $P = 10$ $\mu$W, $T = 300$ K, $\zeta = 2 \times 10^{-5}$ A m and $\omega_m/\kappa_o = 1$.

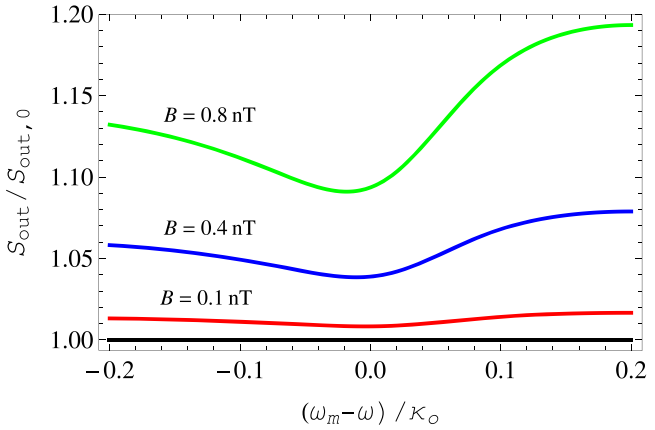


**Figure 3.** The plot shows that sub-nano-Tesla measurement can be made with better resolution if $\omega_m/\kappa_o < 1$. Here we used $\omega_m/\kappa_o = 0.2$, while all the other parameters are the same as in figure 2.

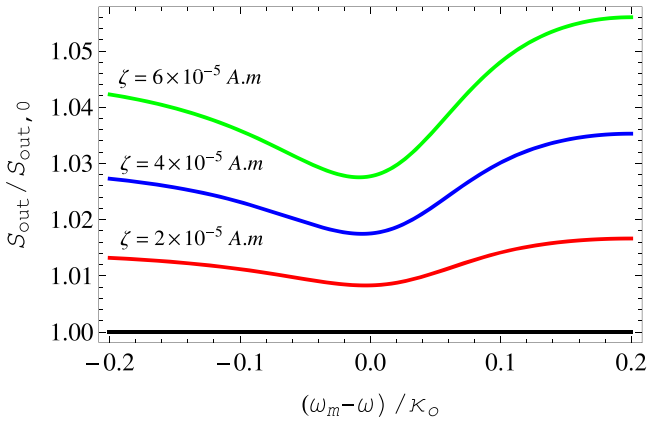


**Figure 4.** The spectral density of the output field for three different choices of current parameter $\zeta$. Here $B = 0.1$ nT while all the other parameters are the same as in figure 3. By increasing the current, the spectral density shifts towards higher values, thus increasing the sensitivity of magnetic field (see figure 3 for comparison).

can be observed in the presence of magnetic field. Figure 2 shows the plot of normalized spectral density $S_{out}/S_{out,0}$ where $S_{out,0}$ represents the output field spectral density when $B$ field is zero. Thus, $S_{out,0}$ represents the total noise floor. We also set the optimum homodyne angle at $\omega = \omega_m$ (i.e. substituting $\omega = \omega_m$ in $\tan\theta_{opt} = \alpha_1$) or equivalently at $\theta_{opt} = \pi/2$ which leads to large dissipative coupling strength [22]. The input power $P = 10$ $\mu$W and the current flowing through the membrane is assumed to be $\zeta = 2 \times 10^{-5}$ A m [11]. The solid straight line at $S_{out}/S_{out,0} = 1$ in figure 2 shows the normalized spectral density of the output field when $B$ field is zero. When $B$ field is turned on, the spectral density of the output field becomes greater than 1, i.e. $S_{out}/S_{out,0} > 1$ and the shift in the spectral density depends upon the strength of the magnetic field. The dip in the spectral density arises due to the membranes fundamental resonance. It may also be noted that shift in the spectral density is large when the detection frequency $\omega < \omega_m$ as compared to the case when $\omega > \omega_m$. However, the system is relatively less sensitive to the magnetic field when the detection frequency is equal or close to the mechanical frequency.

It is interesting to note, if we further shift towards the non-resolved-sideband regime for example, $\omega_m/\kappa_o = 0.2$ as in [24], the spectral density of the output field becomes more sensitive to the magnetic field as shown in figure 3. It may be mentioned that the micro- and nano-optomechanical devices due to their small size, inherently work in the bad cavity regime (i.e. $\omega_m/\kappa_o \ll 1$) [38], which is advantageous for our scheme. By comparing figure 2 and figure 3 it is clear that for $\omega_m/\kappa_o = 0.2$, the shift in the output spectral density is larger even for the magnetic field strength ten times smaller than the results obtained for the case when $\omega_m/\kappa_o \sim 1$.

The measurement sensitivity can be further improved by adjusting the current flowing through the membrane. This is shown in figure 4, where the spectral density of the output field is plotted for three different choices of the current parameter $\zeta$ for $B = 0.1$ nT and $\omega_m/\kappa_o = 0.2$. Our results clearly shows that the sensitivity of the measurement increases by increasing the current through the membrane. However, it may be pointed out that our analysis is based on linearization of the equations of motion around the large mean values (see equations (4)), so for linear approximation to hold, current cannot be increased indefinitely. The linear approximation holds as long as $\eta x \ll 1$, because $\kappa = \kappa_o(1 + \eta x)$ with $x = x_s + \delta x = -\zeta B/(m\omega_m^2) + \delta x$. It is also interesting to note that, due to the topology of MSI, if the current is reversed i.e. $\zeta \to -\zeta$, the position of MO also shifts as $x \to -x$, thus equation (1) remains unchanged and the output spectral density remains the same.

Figure 5 shows a contour plot of the output field spectral density with respect to the magnetic field and current at $\omega = \omega_m$ which is the resonance frequency of the membrane. At $\omega = \omega_m$, the shift in the spectral density is at its minimum (as can be seen in figures 2, 3 and 4). It is clear from figure 5 that for weak magnetic interaction (e.g. $B = 0.1$ nT and $\zeta = 2 \times 10^{-5}$ A m), the shift in the output field spectral density is below 1.01 which can also be verified from figure 4 at $\omega = \omega_m$. The shift in the spectral density enhances when

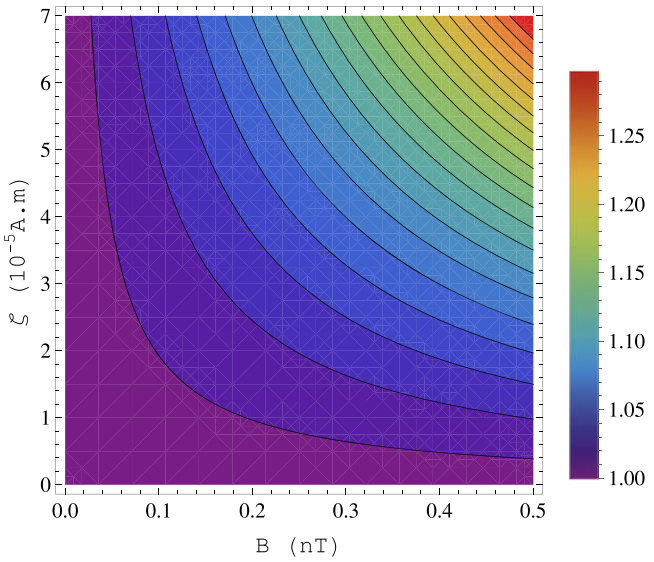


**Figure 5.** Contour plot of the normalized spectral density against $B$ and $\zeta$ at $\omega_m = \omega$. Here $\omega_m/\kappa_o = 0.2$ and all the other parameters are the same as in figure 3.

we increase the current or magnetic field. Thus, for appropriate current values, and detection frequency smaller than the mechanical frequency, and working in the non-resolved-side-band regime, $B$ field upto sub-nano-Tesla levels can be measured by this scheme.

## 4. Conclusion

In conclusion, we have considered a dissipative optomechanical system for the detection of weak magnetic field. In the presence of magnetic field, the position of the membrane depends upon the current flowing through it. Thus by varying the current, the position of the membrane changes which leads to a change in the optical decay rate $\kappa$ or transmissivity of the compound mirror. The effects of change in transmissivity can be seen in the output spectrum of the field. Therefore, by analyzing the spectrum of the output field, weak magnetic field can be measured. Our scheme is based on MSI which to the best of our knowledge is the only proven system for achieving pure dissipative coupling [16, 17]. From experimental point of view, dissipative coupling is more favorable in the micro- and nano-optomechanical devices. The optical line-width for such small devices typically scales inversely with the length of the cavity and eventually results in $\omega_m/\kappa_o \ll 1$, i.e. the so called non-resolved-sideband regime or bad cavity regime. Our proposal works better in this regime and therefore, could be more feasible to detect magnetic field experimentally. Moreover, the system needs no magnetic shielding from the background, as measurements are made relative to the background. This also provides us the liberty to measure even weaker magnetic fields as long as the signal can be resolved from the background. Throughout our numerical simulations, we have used the parameters which are accessible in experiment. Therefore, we believe that our scheme enables potentially practical proposal for precision measurement of weak magnetic field. By adjusting the current and working in the non-resolved-side-band regime, one can make measurement of weak magnetic field upto sub-nano-Tesla levels at room temperature.

## Acknowledgments

A M would like to acknowledge Higher Education Commission of Pakistan for PhD scholarship under Indigenous PhD Fellowship Scheme Phase-II, Batch-III.

## ORCID iDs

Shahid Qamar https://orcid.org/0000-0002-4762-1977

## References

[1] Braginsky V B and Manukin A B 1967 *Sov. Phys. JETP* **25** 653
[2] Braginsky V B, Manukin A B and Yu M 1970 *Tikhonov, Sov. Phys. JETP* **31** 829
[3] Braginsky V B, Gorodetsky M L and Khalili F Y 1997 *Phys. Lett.* A **232** 340
[4] Buonanno A and Chen Y 2002 *Phys. Rev.* D **65** 042001
[5] Aasi J *et al* 2015 *Class. Quantum Grav.* **32** 074001
[6] Braginsky V B and Khalili F Y 1990 *Phys. Lett.* A **147** 251
[7] Braginsky V B, Gorodetsky M L, Khalili F Y and Thorne K S 2000 *Phys. Rev.* D **61** 044002
[8] Vyatchanin S P and Matsko A B 2016 *Phys. Rev.* A **93** 063817
[9] Wu M, Hryciw A C, Healey C, Lake D P, Jayakumar H, Freeman M R, Davis J P and Barclay P E 2014 *Phys. Rev.* X **4** 021052
[10] Forstner S, Prams S, Knittel J, van Ooijen E D, Swaim J D, Harris G I, Szorkovszky A, Bowen W P and RubinszteinDunlop H 2012 *Phys. Rev. Lett.* **108** 120801
[11] Liu Z X, Wang B, Kong C, Si L G, Xiong H and Wu Y 2017 *Sci Rep.* **7** 12521
[12] Zhang J Q, Li Y, Feng M and Xu Y 2012 *Phys. Rev.* A **86** 053806
[13] Marquardt F, Chen J P, Clerk A A and Girvin S M 2007 *Phys. Rev. Lett.* **99** 093902
[14] Wilson-Rae I, Nooshi N, Zwerger W and Kippenberg T J 2007 *Phys. Rev. Lett.* **99** 093901
[15] Elste F, Girvin S M and Clerk A A 2009 *Phys. Rev. Lett.* **102** 207209
[16] Xuereb A, Schnabel R and Hammerer K 2011 *Phys. Rev. Lett* **107** 213604
[17] Sawadsky A, Kaufer H, Nia R M, Tarabrin S P, Khalili F Y, Hammerer K and Schnabel R 2015 *Phys. Rev. Lett.* **114** 043601
[18] Weiss T and Nunnenkamp A 2013 *Phys. Rev.* A **88** 023850
[19] Tarabrin S P, Kaufer H, Khalili F Y, Schnabel R and Hammerer K 2013 *Phys. Rev.* A **88** 023809
[20] Weiss T, Bruder C and Nunnenkamp A 2013 *New J. Phys.* **15** 045017
[21] Agarwal G S and Huang S 2010 *Phys. Rev.* A **81** 041803(R)
[22] Qu K and Agarwal G S 2015 *Phys. Rev.* A **91** 063815
[23] Kilda D and Nunnenkamp A 2016 *J. Opt.* **18** 014007
[24] Huang S and Agarwal G S 2017 *Phys. Rev.* A **95** 023844
[25] Edelstein A 2007 *J. Phys.: Condens. Matter* **19** 165217
[26] Romalis M V and Dang H B 2011 *Mater. Today* **14** 258

[27] Bucholtz F, Dagenais D M and Koo K P 1989 *Electron. Lett.* **25** 1719
[28] Zhai J, Xing Z, Dong S, Li J and Viehland D 2006 *Appl. Phys. Lett.* **88** 062510
[29] Dang H B, Maloof A C and Romalis M V 2010 *Appl. Phys. Lett.* **97** 151110
[30] Wasilewski W, Jensen K, Krauter H, Renema J J, Balabas M V and Polzik E S 2010 *Phys. Rev. Lett.* **104** 133601
[31] Li B B *et al* 2018 *Optica* **5** 850
[32] Walls D F and Milburn G J 1994 *Quantum Optics* (Berlin: Springer)
[33] Thompson J D *et al* 2008 *Nature* **452** 72
[34] Zwickl B M *et al* 2008 *Appl. Phys. Lett.* **92** 103125
[35] Kemiktarak U, Metcalfe M, Durand M and Lawall J 2012 *Appl. Phys. Lett.* **100** 061124
[36] Bagci T *et al* 2014 *Nature* **507** 81
[37] Schmid S *et al* 2014 *J. Appl. Phys.* **115** 054513
[38] Bennett J S *et al* 2016 *New J. Phys.* **18** 053030